# Low Cost Flux-Switching Brushless AC Machines

J. T. Chen[1], Z. Q. Zhu[1], S. Iwasaki[2], and R. Deodhar[2]
[1]Department of Electronic and Electrical Engineering, University of Sheffield, Sheffield S1 3JD, U.K.
[2]IMRA Europe S.A.S., U.K. Research Centre, Brighton BN1 9RS, U.K.
J.Chen@sheffield.ac.uk, Z.Q.Zhu@sheffield.ac.uk, SI@imra-ukrc.com, and RD@imra-ukrc.com

*Abstract*- **A low cost 3-phase DC winding excited flux-switching (FS) brushless AC machine is developed from the FS permanent magnet (FSPM) machine. The influence of stator and rotor pole number combination on its electromagnetic performance, including flux-linkage and back-emf waveforms, electromagnetic static torque, and torque-current density characteristics, are predicted by 2-D finite element analyses and validated by experiment. In addition, the torque capability of the FS machine and FSPM machines with rare earth and ferrite magnets, respectively, are compared by the finite element analyses. It is found that whilst it is low cost, the torque capability in the FS machine may be limited by the significant magnetic saturation in the stator teeth.**

## I. Introduction

Although permanent magnet (PM) machines exhibit high torque density and high efficiency, the rare earth magnet material, e.g. NdFeB, is expensive and the working environmental temperature may limit its application. In addition, the flux-weakening operation at high speed is relatively difficult for PM machines due to fixed PM excitation. In order to reduce the cost, one of the possible solutions is to replace the magnet excitation by the DC winding excitation.

The conventional DC winding excited synchronous machine employs the field winding on the rotor, and, consequently, the slip-rings are required to supply the field current. Recently, the PM machines having magnets on the stator, viz. doubly salient, flux-reversal, and flux-switching (FS) PM machines, were developed, and the excitation of magnetic field may be realized by the DC winding. Hence, DC winding excited brushless machines can be realised by placing the field winding on the stator. The DC winding excited doubly salient machine was proposed in [1], and the hybrid excited doubly salient [2, 3] and FS [4] PM machines were investigated. In addition, a DC winding excited FS machine with modular rotor and non-overlapping windings was recently investigated in [5-7]. Although, in [8], it was mentioned that the magnets could be replaced by the DC windings in 3-phase FS PM (FSPM) machines, the DC winding excited 3-phase FS machine was not further investigated.

The 1-phase DC winding excited FS machine and its controller were proposed and analyzed [9] for automotive application due to extremely low cost of the machine and drive system [10]. Since the field winding is excited by unipolar current, it can be directly connected in parallel or in series with the power converter which feeds the bipolar current into the armature winding. The design principle was given in [11], and the 1-phase FS machine was shown to exhibit a higher output power density than the equivalent universal and induction machines, and comparable efficiency to that of the induction machine. However, the 1-phase machine has problems of low starting torque, large torque ripple, and fixed rotating direction.

The 3-phase DC winding excited FS machine is investigated in this paper since its cost is extremely low. The FS machine to be investigated is developed from the 12/10 stator/rotor pole FSPM machine [12]. Unlike the FS machine with non-overlapping windings [5-7] and FSPM machine having segmented rotor and stator cores, respectively, the stator and rotor laminations of the developed FS machine are similar to those of a switched reluctance machine, although the stator winding is different.

In this paper, the operation principle of the 3-phase FS machine is described. The influence of design parameters and rotor pole number on the electromagnetic performance of FS machines is investigated and validated by experiments. The torque capability of the FS machine and FSPM machines with rare earth and ferrite magnets are compared by the finite element (FE) analyses, with particular emphasis on the influence of magnetic saturation.

## II. Topologies of DC Winding Excited FS Machines

It is well-known that the magnetic potential source of permanent magnets can be physically modelled by the surface current, as shown in Fig. 1(b). However, this is not possible to realise in practice and can usually be achieved by using the volume current, Fig. 1(c). Therefore, the DC winding excited FS machine can be directly obtained from the corresponding FSPM machine, Fig. 2(a), by replacing the magnets with the volume winding excited model, Fig. 2(b). It should be noted that there is a lamination steel core in the middle of DC winding excited model to increase the permeance and to link the stator "U"-shaped lamination steel segments as a complete stator. However, the field produced by the DC field conductors at the outer surface of the stator goes through outside of the stator instead of the rotor. Hence, the DC field conductors close to the outer surface of the stator can be removed to enlarge the slot area for the field conductors close to the air-gap which produces the main flux, Fig. 2(c), and the DC field conductors can also be connected in an alternative way as illustrated in Fig. 2(d) to reduce the number of coils. When the influence of end-effect and end winding is ignored, the machines having two kinds of DC field conductor connections exhibit the same electromagnetic performance, and hence this machine, Fig. 2(d), is further investigated. Similar to the FSPM machine, the conductors in one DC field winding slot and its adjacent two stator teeth compose one stator pole, as illustrated in Fig.2 for 12-stator pole machines.

978-1-4244-8218-4/10/$26.00 ©2010 Crown

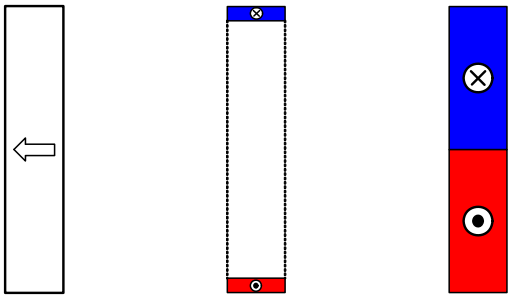

(a) (b) (c)

Fig. 1. Surface and volume current models for potential source of permanent magnets. (a) Permanent magnet. (b) Surface current model. (c) Volume current model.

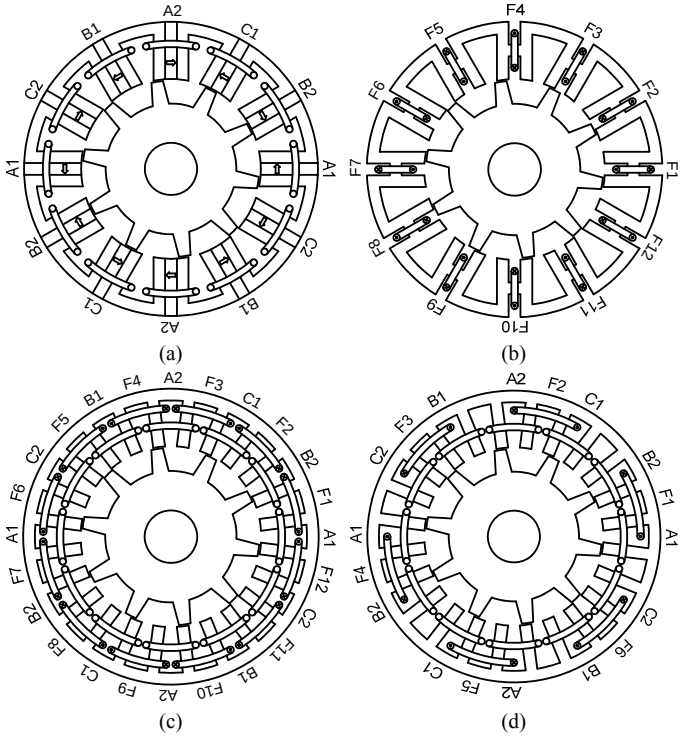

(a) (b) (c) (d)

Fig. 2. 12/10 stator/rotor pole FSPM and DC winding excited FS machines. (a) FSPM machine. (b) FS machine I. (c) FS machine II. (d) FS machine III.

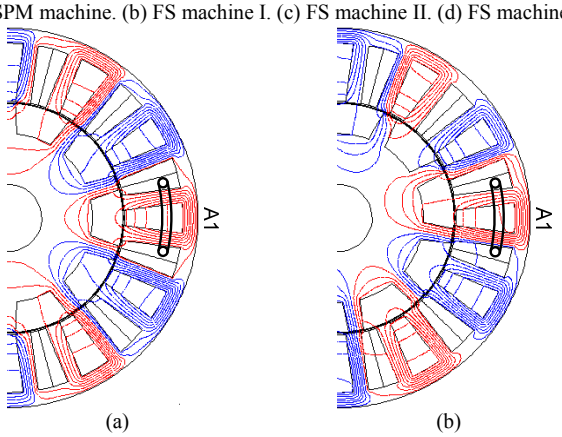

(a) (b)

Fig. 3. Open-circuit field distributions. (a) Rotor at q-axis, flux-linkage of phase A = 0. (b) Rotor at d-axis, flux-linkage of phase A = max.

The open-circuit field distribution of the FS machine is shown in Fig. 3. Similar to the FSPM machine, when the rotor rotates by a quarter of rotor pole pitch, the main flux of coil A1 varies from zero to maximum, i.e. from Figs. 3(a) to (b), and then the back-emf is produced.

## III. Influence of Design Parameter on Electromagnetic Torque

The original design parameters of a 12/10 stator/rotor pole FS machine are given in Table I. It has equal stator tooth width, stator back-iron thickness and rotor pole width. The machine is designed to have very high overload capability. Hence, a significantly large field current density of 20A/mm$^2$ (winding packing factor = 1) is employed to optimize the machine in this section. However, the rated current density is ~4.5A/mm$^2$.

TABLE I
Major Parameters of Original Reference FS Machines

| | | | |
|---|---|---|---|
| Number of phases | 3 | Stator back-iron thickness | 4.4 mm |
| Outer radius of stator | 45 mm | Rotor tooth width | 4.4 mm |
| Inner radius of stator | 29.75 mm | Number of turns/phase | 72 |
| Airgap length | 0.5 mm | Number of DC winding turns | 144 |
| Active axial length | 25 mm | | |
| Stator tooth width | 4.4 mm | Rated speed | 400 rpm |

### A. Split ratio

Firstly, the variation of electromagnetic performance with split ratio is investigated since the split ratio is a key parameter in machine design. It should be noted that the slot area varies with the split ratio. The 2-D FE predicted average electromagnetic torque is shown in Fig. 4. The torque varies significantly with split ratio, and the optimized torque-current density characteristic is obtained when the split ratio is 0.65 which is larger than that of the FSPM machine, being 0.6. Hence, the machine with the optimized split ratio of 0.65 is used as a reference machine for further optimizing other parameters.

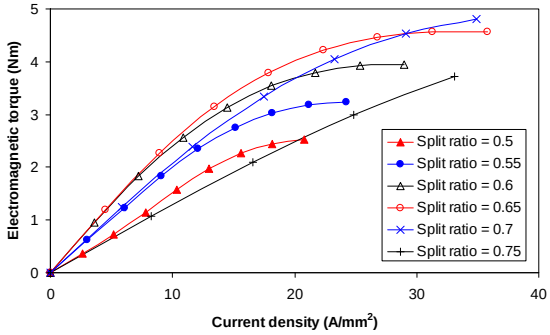


Fig. 4. Torque-current density characteristics of FS machine with different split ratio, $I_d$=0.

### B. Stator tooth bottom width

As will be shown later, the magnetic saturation at the bottom of stator tooth in the FS machine is much heavier than that of the conventional FSPM machine. Although the whole stator tooth width can affect the magnetic saturation, it affects the air-gap field distribution as well. In order to reduce the magnetic saturation and maintain the air-gap field distribution, the bottom width of stator tooth is optimized by 2-D FE analyses, and the open-circuit and load field distributions of the machine with trapezoid stator teeth are shown in Fig. 5. From the torque-current density characteristics as shown in Fig. 6, the optimized bottom width of stator tooth is 1.2 times of the original width. It should be noted that only three curves are given in Fig. 6 in order to show them clearly.

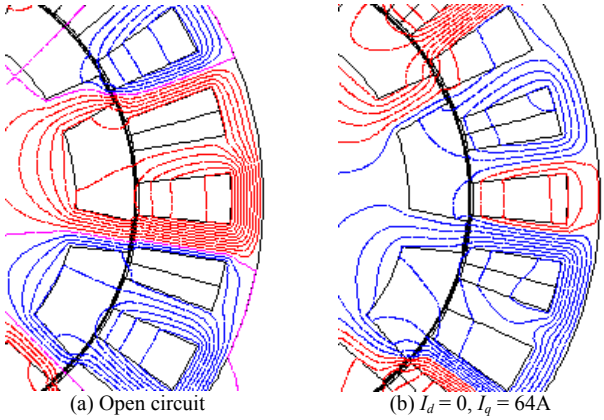

(a) Open circuit (b) $I_d = 0$, $I_q = 64$A

Fig. 5. Field distributions of FS machine when bottom width of stator tooth is 1.2 times of original width, $J_f = 20$A/mm$^2$.

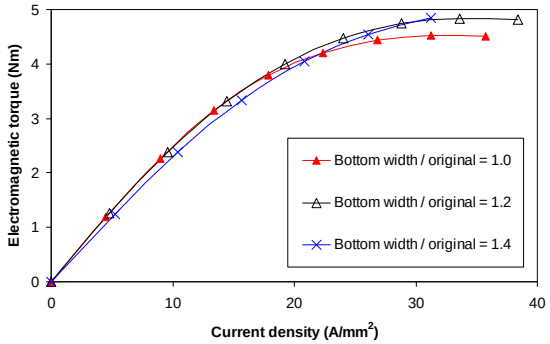


Fig. 6. Torque-current density characteristics of FS machines with different bottom width of stator tooth, $I_d = 0$.

### C. *Field to armature winding slot area ratio*

The field and armature windings perform different functions, and their slot areas may be different for maximum torque. The optimized field winding slot area was less than the armature winding slot area for the 1-phase DC winding excited FS machine with armature winding being bifilar configuration for low cost controller [13].

When the total slot area is fixed, the ratio of slot area for field and armature windings can be optimized for minimum copper loss. Ignoring the influence of end winding, the copper loss in the 3-phase FS machine can be given by:

$$P_{cua} = 3I_a^2 R_a = \left(J_a S_a k_{pa}\right)^2 \frac{\rho_{cu} L_a N_s}{S_a k_{pa}} = \rho_{cu} L_a N_s \cdot S_a k_{pa} J_a^2 \quad (1)$$

$$P_{cuf} = I_f^2 R_f = \left(J_f S_f k_{pf}\right)^2 \frac{\rho_{cu} L_a N_s}{S_f k_{pf}} = \rho_{cu} L_a N_s \cdot S_f k_{pf} J_f^2 \quad (2)$$

$$P_{cu} = P_{cua} + P_{cuf} = \rho_{cu} L_a N_s \left(S_a k_{pa} J_a^2 + S_f k_{pf} J_f^2\right) \quad (3)$$

where $P_{cua}$ and $P_{cuf}$ are the copper loss of the armature and field windings (W), $P_{cu}$ is the total copper loss including copper loss of armature and field windings (W), $I_a$ is the phase current (A, rms), $R_a$ is the phase resistance (Ω), $J_a$ and $J_f$ are the current density of armature and field windings (A/mm$^2$, rms), $S_a$ and $S_f$ are slot area of armature and field windings (mm$^2$), $k_{pa}$ and $k_{pf}$ are the packing factor of armature and field windings, $\rho_{cu}$ is the electrical resistively of copper (Ωmm), $L_a$ is the active length of the machine (mm), and $N_s$ is the number of stator poles. If the influence of magnetic saturation is ignored, the electromagnetic torque $T_e$ is proportional to the armature current and DC excitation current, viz.:

$$T_e = k_e S_a k_{pa} J_a S_f k_{pf} J_f \quad (4)$$

where $k_e$ is constant, which is determined by the dimensions of the machines. (4) can be rewritten as:

$$J_f = \frac{T_e}{k_e S_a k_{pa} J_a S_f k_{pf}} \quad (5)$$

Hence, the copper loss can be obtained by substituting (5) into (3):

$$P_{cu} = \rho_{cu} L_a N_s \left( S_a k_{pa} J_a^2 + \frac{T_e^2}{k_e^2 S_a^2 k_{pa}^2 J_a^2 S_f k_{pf}} \right) \quad (6)$$

In order to minimize the copper loss with fixed electromagnetic torque, the current density for armature winding can be obtained from the equation:

$$\frac{\partial P_{cu}}{\partial J_a} = 0 \quad (7)$$

i.e.

$$J_a = \sqrt[4]{\frac{T_e^2}{k_e^2 \left(S_a k_{pa}\right)^3 S_f k_{pf}}} \quad (8)$$

The current density of field winding can also be obtained according to (5):

$$J_f = \sqrt[4]{\frac{T_e^2}{k_e^2 \left(S_f k_{pf}\right)^3 S_a k_{pa}}} \quad (9)$$

Then the corresponding copper loss of the armature and field windings can be given by:

$$P_{cua} = P_{cuf} = \rho_{cu} L_a N_s \frac{T_e}{k_e \sqrt{S_a k_{pa} S_f k_{pf}}} \quad (10)$$

Hence, the minimum copper loss can be obtained when the copper loss of armature windings equals to that of field windings. When the total slot area $S_t = N_s(S_a + S_f)$ is constant, the slot area of armature and field windings can be optimized for minimum copper loss as:

$$\frac{\partial P_{cua}}{\partial S_a} = \frac{\partial \left( \rho_{cu} l_a N_s \dfrac{T_e}{k_e \sqrt{S_a k_{pa} \left(S_t / N_s - S_a\right) k_{pf}}} \right)}{\partial S_a} = 0 \quad (11)$$

i.e.

$$S_a = S_f = \frac{S_t}{2N_s} \quad (12)$$

Therefore, the minimum copper loss can be obtained when the slot area of armature winding equals to that of field winding. Moreover, the optimized field current density should be equal to the armature current density (rms) when their winding packing factors are equal according to (8), (9), and (12).

However, the optimized ratio of slot area for field and armature windings may change due to magnetic saturation. Hence the slot area ratio is further optimized by 2-D FE analyses. In order to maintain the air-gap field distribution, the slot area ratio of the machine with fixed position of stator teeth close to the air-gap, Fig. 7(a), viz. equal slot opening for field and armature winding slots, is firstly optimized. The torque-current density characteristics with different slot area ratio are compared in Fig. 8, and the optimized slot area ratio

is 1 in the entire electric loading region, which validates the analytical result. On the other hand, the slot area ratio of the machine when the slot opening varies with the corresponding slot area, viz. the stator teeth being radial, Fig. 7(b), is optimized as well. Again, the torque-current density characteristics are shown in Fig. 9. The largest torque is obtained by the machine having the slot area ratio = 1 when the current density is small. However, the torque of the machine with small slot area ratio saturates earlier than that of the machine with larger slot area ratio. The optimized slot area ratio is 1.26 in the entire electric loading region. It should be noted that the torque-current density characteristic when the slot area ratio is 1 is the optimized result by assuming equal slot opening, which is slightly lower than that optimized result with unequal slot opening.

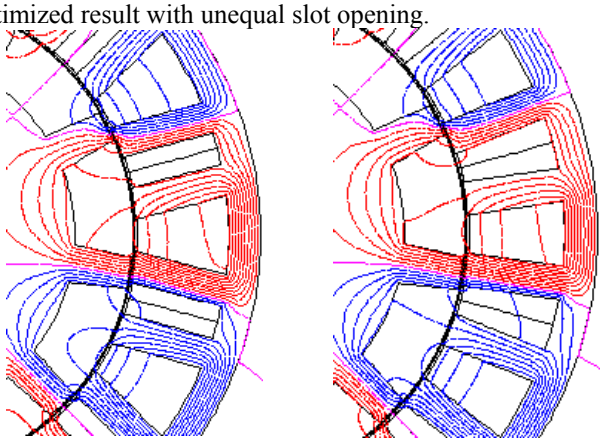

(a) Equal slot opening (b) Unequal slot opening

Fig. 7. Open-circuit field distributions of FS machine with equal and unequal slot opening and different slot areas for field and armature windings.

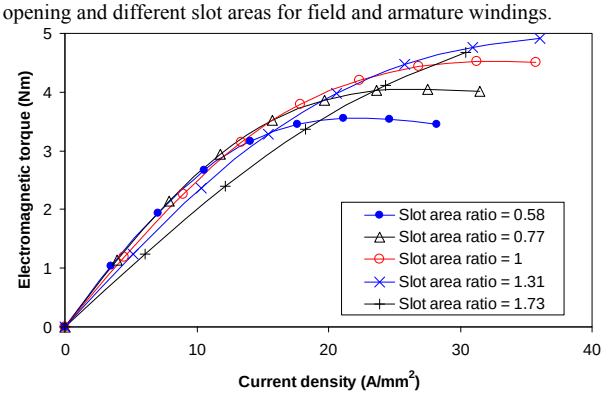


Fig. 8. Torque-current density characteristics of FS machines with different slot area ratio and fixed slot opening, $I_d = 0$.

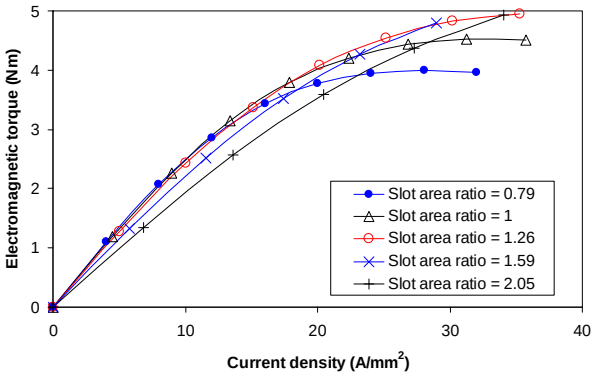


Fig. 9. Torque-current density characteristics of FS machines with different slot area ratio and stator teeth being radial, $I_d = 0$.

### *D. Other design parameters*

The other design parameters, such as stator back-iron thickness and stator tooth top width etc., are optimized for maximum torque capability, and are summarized in Table II.

TABLE II
MAJOR DESIGN PARAMETERS OF FS AND FSPM MACHINES

| | FS machine | FSPM machine |
|---|---|---|
| Number of phase | 3 | |
| Number of stator poles | 12 | |
| Number of rotor poles | 10, 11, 13, 14 | 10 |
| Outer radius of stator | 45 mm | |
| Active axial length | 25 mm | |
| Air-gap length | 0.5 mm | |
| Inner radius of stator | 29.75 mm | 27.5 mm |
| Stator tooth top width | 4.4 mm | 3.6 mm |
| Stator tooth bottom width | 4.7 mm | 3.6 mm |
| Stator yoke thickness | 3.5 mm | 3.6 mm |
| Slot opening for armature winding | 3.8 mm | 3.6 mm |
| Slot opening for DC winding | 5.0 mm | -- |
| Rotor tooth width | 5.6 mm | 3.6 mm |
| Number of phase turns | 48 | 72 |
| Number of DC winding turns | 144 | -- |
| PM thickness | -- | 3.6 mm |
| Magnetic remanence | -- | 1.2 T |
| Relative PM permeability | -- | 1.05 |
| Rated speed | 400 rpm | |

## IV. COMBINATION OF STATOR AND ROTOR POLE NUMBERS

Similar to FSPM machines, there are a lot of feasible stator and rotor pole number combinations in the FS machines. For simplicity, a 12-pole stator is employed, and, hence, 10-, 11-, 13-, and 14-rotor pole machines are analyzed since the optimized rotor pole number is close to the stator pole number in the conventional FSPM machines [14]. The electromagnetic performance of the 12/10, 12/11, 12/13, and 12/14 stator/rotor pole DC winding excited FS machines are predicted by 2-D FE analyses and compared. Their major parameters are given in Table II. The number of turns per phase is 48, and the DC winding turns is 3×48=144. The optimized rotor pole width is 1/3 rotor pole-pitch.

### *A. Flux-linkage and Back-emf Waveforms*

The variations of the flux-linkage and back-emf waveforms with the rotor pole numbers are showen in Fig. 10. The back-emf waveforms of the FS machines are sinusoidal. The flux-linkage reduces with the increase of rotor pole number, while the 13- and 14-rotor pole machines exhibit similar back-emf and is larger than those of the 10- and 11-rotor pole machines due to higher electrical frequency, which is consistent with the FSPM machines [14].

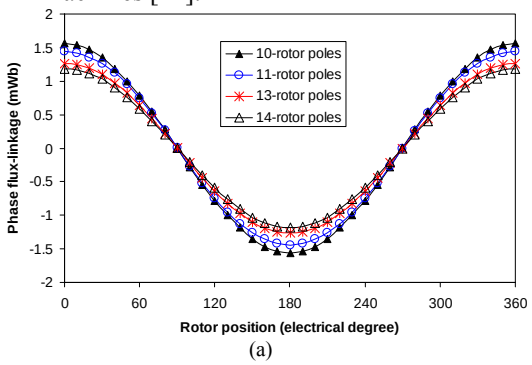


(a)

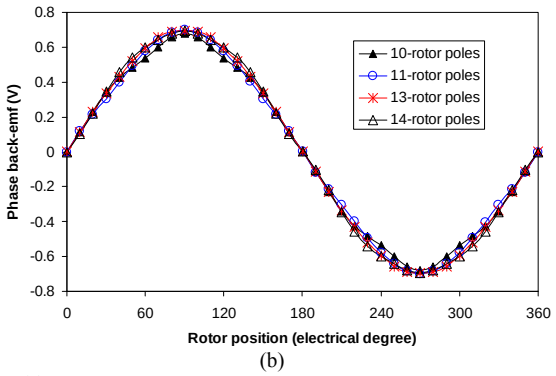


(b)

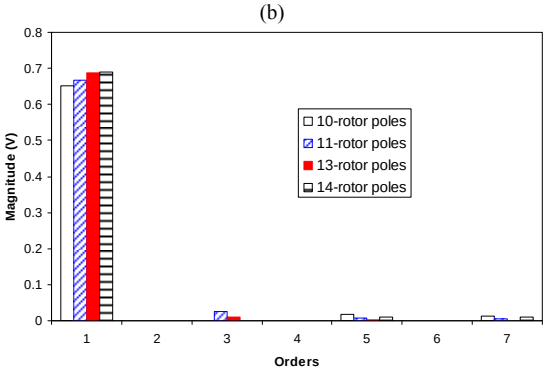


(c)

Fig. 10. Flux-linkage and back-emf waveforms of FS machines, DC excitation current $I_f$=10A. (a) Phase flux-linkages. (b) Phase back-emfs, 400rpm. (c) Spectra of phase back-emfs, 400rpm.

### *B. Electromagnetic Torque*

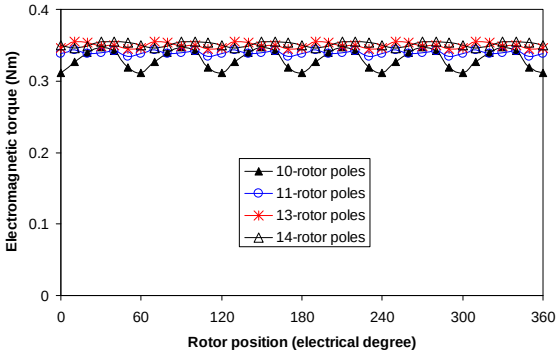


Fig. 11. Torque waveforms of FS machines, BLAC operation, DC excitation current $I_f$=10A, $I_d$=0, and $I_q$=14.1A.

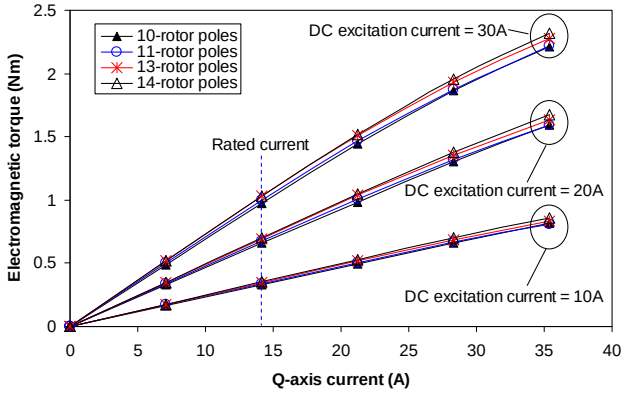


Fig. 12. Average torque-current characteristics of FS machines, BLAC operation, $I_d$=0.

The torque waveforms of the FS machines with different rotor pole numbers are shown in Fig. 11. Furthermore, Fig. 12 compares the torque-current characteristics. The 11-, 13-, and 14-rotor pole machines exhibit similar torque ripple, which is significantly lower than that of the 10-rotor pole machine which also has the lowest torque. The 13- and 14-rotor pole machines exhibit similar torque capability which is larger than those of the 10- and 11-rotor pole machines due to higher back-emfs.

## V. Combination of Torque Capability between DC Winding Excited FS and FSPM Machines

The electromagnetic performance of 12/10 stator/rotor pole DC winding excited FS and FSPM machines are predicted by 2-D FE analyses and compared, Fig. 13. Both machines have the same outer diameter and active axial length. Their major parameters are compared in Table II.

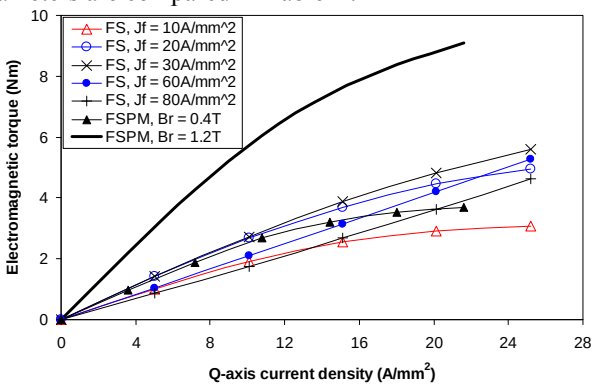


Fig. 13. Comparison of torque-current density characteristics of FSPM and FS machines with different DC excitation current densities $J_f$, winding packing factor=1 and $I_d$ = 0.

Only when the FS machine with $J_f$ = 20A/mm$^2$ (winding packing factor=1), it will exhibit slightly larger torque than that of the FSPM machine when $B_r$ = 0.4T (ferrite magnets). Therefore, FSPM machine when $B_r$ = 1.2T (NdFeB magnets), exhibits significantly larger torque capability than that of the FS machine even when a very large DC field current is applied, which is due to different magnetic saturation in stator teeth in two machines. As can be seen from Fig. 14, the main flux in the FS machine is through the stator tooth from the top to the bottom, but it is only partly through the stator tooth in the FSPM machine. Hence, the whole teeth are saturated magnetically in the FS machine, while it is only partly saturated in the FSPM machine. This is why even when a very large field current is employed, the FS machine still exhibits much lower torque than that of the FSPM machine employing NdFeB magnets.

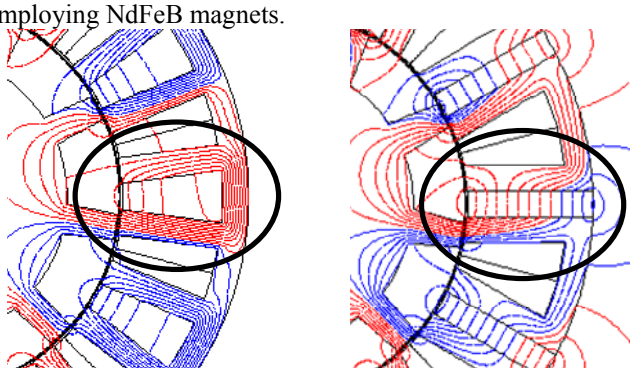

(a) (b)

Fig. 14. Comparison of open-circuit field distributions of FS and FSPM machines. (a) FS machine. (b) FSPM machine.

## VI. Experimental Validation

The electromagnetic performance of the 12/10, 12/11, and 12/13 stator/rotor pole FS prototype machines, Fig. 15, is measured and compared with those predicted by 2-D FE analyses. The design parameters are given in Table II. The 2-D FE predicted back-emf waveform and torque-current characteristic agree well with measured results, Figs. 16 and 17. The static torque is measured by supplying the DC to phase A with phases B and C parallel connected ($I_b$=$I_c$=-$I_a$/2) when the rotor is at q-axis. It is worth to mention that the torque in Figs. 12 and 13 is the average value, while Fig. 17 shows the torque when the rotor is at q-axis.

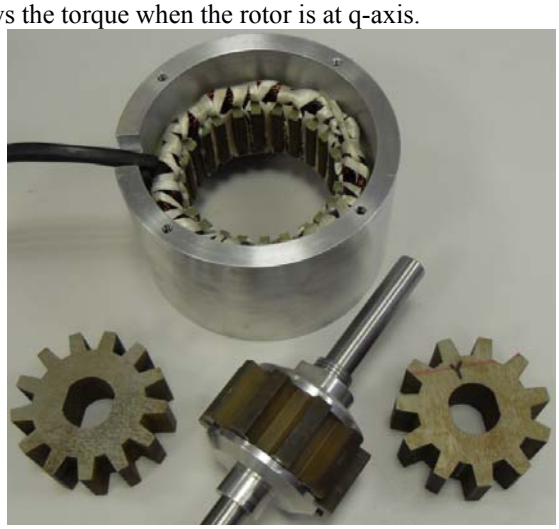

Fig. 15. 12/10, 12/11, and 12/13 stator/rotor pole FS prototype machines.

## VII. Conclusions

Low cost 3-phase DC winding excited FS machine is developed from the FSPM machine by employing the DC winding excitation to replace the magnet excitation. The 12/13 and 12/14 stator/rotor pole machines exhibit similar back-emf and torque, which are higher than those of the 12/10 and 12/11 stator/rotor pole machines. Whilst it is low cost, the DC winding excited FS machine exhibits significantly lower torque than that of the FSPM machine having either NdFeB magnets or even ferrite magnets. It is mainly due to the main flux is through the whole stator tooth in the FS machine, while it is only partly through the stator tooth in the FSPM machine, viz. different magnetic saturation in the stator teeth.

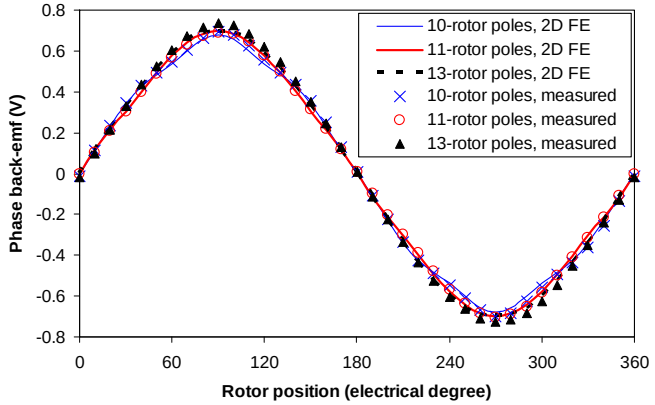


Fig. 16. Comparison of 2-D FE predicted and measured phase back-emf waveforms of FS prototype machine, DC excitation current=10A, 400rpm.

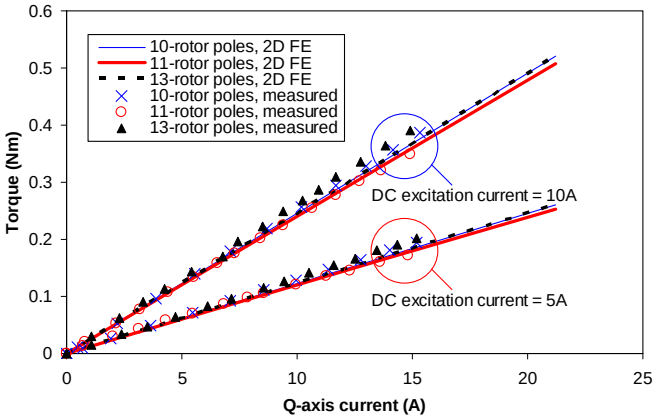


Fig. 17. Comparison of 2-D FE predicted and measured torque-current characteristics of FS prototype machine, $I_d$=0 rotor being at q-axis.

## References


[1] Y. Fan, K. T. Chau, and S. Niu, "Development of a new brushless doubly fed doubly salient machine for wind power generation," *IEEE Trans. Magnetics*, vol. 42, no. 10, pp. 3455-3457, Oct. 2006.

[2] Y. Li and T. A. Lipo, "A doubly salient permanent magnet motor capable of field weakening," *Proc. IEEE Power Electronics Specialists Conf.*, vol. 1, June 1995, pp. 565-571.

[3] K. T. Chau, M. Cheng, and C. C. Chan, "Nonlinear magnetic circuit analysis for a novel stator doubly fed doubly salient machine," *IEEE Trans. Magnetics*, vol. 38, no. 5, pp. 2382-2384, Sept. 2002.

[4] E. Hoang, M. Lecrivain, and M. Gabsi, "A new structure of a switching flux synchronous polyphased machine with hybrid excitation," *Proc. Eur. Conf. Power Electronics and Applications*, Sept. 2007, pp. 1–8.

[5] Shinji Nishimura, "Dynamo-electric machine," *United States Patent*, US 6,495,941, Dec. 2002.

[6] S. Iwasaki, and R. Deodhar, "An electrical machine," *UK Patent*, GB0904690.1, Mar. 2009.

[7] A. Zulu, B. Mecrow, and A. Armstrong, "A wound-field three-phase flux-switching synchronous motor with all excitation sources on the stator," *Proc. IEEE Energy Conversion Congress and Exposition (ECCE2009)*, San Jose, USA, 20-24 September, 2009, pp. 1502-1509.

[8] E. Hoang, A. H. Ben-Ahmed, and J. Lucidarme, "Switching flux permanent magnet polyphased synchronous machines," *Proc. 7th Eur. Conf. Power Electronics and Applications*, vol. 3, 1997, pp. 903–908.

[9] C. Pollock, and M. Wallace, "The flux switching motor, a DC motor without magnets or brushes," *in Proc. IEEE Industry Application Society Annu. Meeting*, vol. 3, 1999, pp. 1980–1987.

[10] C. Pollock, H. Pollock, R. Barron, J. R. Coles, D. Moule, A. Court, and R. Sutton, "Flux-switching motors for automotive applications," *IEEE Tran. Ind. Appl.*, vol. 42, no. 5, pp. 1177-1184, Sept./Oct. 2006.

[11] J. F. Bangura, "Design of high-power density and relatively high-efficiency flux-switching motor," *IEEE Trans. Ener. Conv.*, vol. 21, no. 2, pp. 416-425, June 2006.

[12] Z. Q. Zhu, Y. Pang, D. Howe, S. Iwasaki, R. Deodhar, and A. Pride, "Analysis of electromagnetic performance of flux-switching permanent magnet machines by non-linear adaptive lumped parameter magnetic circuit model," *IEEE Trans. Magnetics*, vol.41, no.11, pp.4277-4287, 2005.

[13] H. Pollock, C. Pollock, R. T. Walter, and B. V. Gorti, "Low cost, high power density, flux switching machines and drives for power tools," *in Proc. IEEE Industry Application Society Annu. Meeting*, Oct. 2003, pp.1451–1457.

[14] J. T. Chen, and Z. Q. Zhu, "Winding configurations and optimal stator and rotor pole combination of flux-switching pm brushless ac machines," *IEEE Trans. Energy Conversion*. in press.